Chain Orientation and Distribution in Ring-Banded Spherulites Formed in Poly(ester urethane) Multiblock Copolymer

WEI WANG, YING JIN, XIAONIU YANG, ZHAOHUI SU

State Key Laboratory of Polymer Physics and Chemistry, Changchun Institute of Applied Chemistry, Graduate School of Chinese Academy of Sciences, Chinese Academy of Sciences, Changchun 130022, People's Republic of China

Received 7 September 2009; revised 22 November 2009; accepted 24 November 2009
DOI: 10.1002/polb.21919
Published online in Wiley InterScience (www.interscience.wiley.com).

ABSTRACT: A poly(ester urethane) multiblock copolymer containing poly(ε-caprolactone) glycol (PCL) soft segments gives ring-banded spherulite as crystallized from its melted film. Analysis based on polarized light microscopy and atomic force microcopy revealed that the ring-banded structures consist of alternate convex and concave bands as a consequence of rhythmic growth. These convex and concave bands, which are composed of flat-on and edge-on lamellae, show layered terrace-like and fibrillar morphology, respectively. The chain orientation and composition distribution in the ring-banded spherulites were further investigated using FTIR imaging. The convex bands are mainly PCL-rich domains with perpendicular chain orientation to the substrate, and the concave bands are urethane-rich domains, where the PCL chains are perpendicular to the radial growth directions of the spherulite but parallel to the film plane. The formation of different orientations in the convex and concave bands is attributed to the rhythmic growth behavior for the copolymers with composition distribution along the chains. © 2010 Wiley Periodicals, Inc. J Polym Sci Part B: Polym Phys 48: 541–547, 2010

KEYWORDS: block copolymers; FTIR; orientation; ring-banded spherulite

INTRODUCTION Shape-memory polymers (SMPs) have attracted significant attention among both industrial and academic researchers for their potential applications in various areas, such as smart fabrics,[1] minimally invasive surgery,[2,3] and intelligent medical devices.[4] SMP belongs to the group of "actively moving polymers" and is able to remember and recover its permanent shape after shape deformation under certain stimulus such as heat or light.[5–13] The shape-memory effect is based on the microstructures of the polymers including molecular architecture and phase configuration.[9–11] SMPs are elastic polymer networks accompanied by stimuli-sensitive switches and consist of two components, netpoints and switching segments.[9–11] The netpoints determine the permanent shape and can be achieved by either chemical (covalent bonds) or physical (intermolecular interactions) nature, imparting a level of rigidity and dimensional stability. The switching segments are associated with the temporary shape and can be either amorphous or crystalline. An important class of heat-stimulus SMPs is segmented polyurethanes, most of whose switching segments are amorphous polyesters or polyethers. However, crystalline switching segments have also been introduced into segmented polyurethane SMPs recently due to its specialty of high crystalline soft segment.[7–11,13] Poly(ε-caprolactone) (PCL) is often introduced into SMPs as the crystalline switching segments, so that the SMPs become biodegradable and are expected to have applications in medical devices.[2,7,10] The crystalline structure of the switching segments in SMPs plays an important role and affects the morphology and shape-memory effects of the SMPs.[7,14] The crystalline structures of PCL homopolymer or copolymers and their blends with other polymers have been studied extensively during past decades. Neat PCL shows ring-banded structures only when crystallized at temperatures very close to its melting temperature, which will take an extremely long time. In contrast, PCL in its miscible blends can exhibit ring-banded spherulites in a quite wide temperature range.[15–18] In addition, PCL copolymers like PCL-*b*-PEG also exhibit ring-banded spherulites.[19]

A ring-banded spherulite exhibits a concentric rings or bands under polarized light microscopy (PLM), and it is a common morphological feature in many kinds of materials such as inorganic matters,[20,21] liquid crystals,[21,22] and polymers.[22–26] It is generally believed that the formation of ring-banded structure is attributed to periodic twisting of lamellar crystals along the radial growth direction of the spherulite.[23] Various mechanisms of the lamellar twisting have been proposed.[22–34] Lotz and Cheng published a comprehensive review on the lamellar twisting by the unbalanced surface stress,[22] and structural discontinuities caused by isochiral dislocation was proposed by Keith and Padden.[24] In addition, Kyu et al. have suggested that banded spherulites exhibit

Correspondence to: Z. Su (E-mail: zhsu@ciac.jl.cn)

concentric bands and rhythmic growth.[25,26] Although it has been studied for decades, there seems no rules between polymer structure and the formation of ring-banded spherulites.

There are various characterization methods to reveal the lamellar orientation and formation mechanisms of ring-banded spherulites such as PLM, atomic force microscopy (AFM),[30–34] electron microscopy (EM),[22,27,29,35] secondary ion mass spectroscopy (SIMS),[16,30,36] and microfocus X-ray diffraction (XRD).[37,38] Although these methods can provide extensive information on ring-banded spherulites, they cannot discriminate the bulk composition and orientation of amorphous chains between the two bands. FTIR imaging combines a focal plane array detector with an infrared microscope and is able to provide simultaneous collection of spatial and spectral information, thus it could assess both morphology and chemical compositions.[39–41] The use of polarized radiation for the production of FTIR images, first reported by Koenig and coworker[39] and Wilhelm and coworker[40] can provide the combination of morphology and molecular chain orientations for both crystalline and amorphous domains.

In this study, we use PLM, AFM, and FTIR imaging to investigate ring-banded spherulites of a poly(ester urethane) (PEU) multiblock copolymer and reveal the spherulite morphology, composition distribution, and chain orientation within the ring-banded spherulite. This may provide helpful information for further mechanism study and design of SMPs.

EXPERIMENTAL

Sample Preparation

A PEU multiblock copolymer with PCL as the soft segments (switching segments in the SMP), 2,4-toluene diisocyanate (TDI)-ethylene glycol (EG) as the hard segments (netpoints in the SMP), whose structure shown in Scheme 1, was used in this study. Details of its synthesis and characterization have been reported previously.[7] The M_n of the PCL soft segment was 10,000 g/mol, and the PEU composition was PCL:TDI:EG = 1:7:6. Thin films of the PEU were prepared by casting a chloroform solution onto glass plates, which were maintained under vacuum at 40 °C for 12 h to remove the residual chloroform. The thickness of the film was within 5 μm. The film was placed on a hot stage, melted at 90 °C under nitrogen purge for 5 min to erase the thermal history, and then, quickly cooled to 48 °C and annealed for 48 h. The film was studied using PLM, AFM, FTIR imaging.

Instrumentation

PLM observations of the thin films were performed using a Leica DMLP microscope equipped with a Linkam THMS 600 hot-stage. Spherulite growth images as a function of time were recorded under transmission light with a CCD camera.

AFM studies were performed using a SPA-300HV atomic force microscope coupled with a SPI 3800*N* controller (Seiko Instruments Industry Co.). Probes with a resonant frequency of 60–150 kHz and a spring constant of 3 *N*/m were used. A 150 μm scanner was selected, and the tapping mode was used to obtain height and phase images.

Thin films were transferred from glass plates to CaF_2 plates for FTIR imaging measurements, which were carried out on a Bruker imaging system consisting of an IFS 66v/s FTIR spectrometer coupled with a Hyperion 3000 infrared microscope equipped with a 64 × 64 (4096) mercury cadmium telluride (MCT) focal plane array (FPA) detector. Images were collected in transmission mode for a sample area of 256 × 256 μm^2 (with a 15× objective) with 128 scans coadded at a resolution of 8 cm^{-1} in the range of 3900–900 cm^{-1}. For polarized measurements, spectra were collected from the identical area with radiation polarized parallel and perpendicular, respectively. Data were processed using the Bruker OPUS 6.5 software. To monitor the chain orientation within the spherulites, the $\nu(CH_2)$ and δ(NH) absorption bands were selected to calculate the orientation functions of the PCL soft segments (SS) and the hard segments (HS), respectively. As the $\nu(CH_2)$ and δ(NH) bands have dipoles perpendicular and parallel to the chain axis, respectively, the orientation functions were calculated by the following formulae,[42]

$$f_{SS} = -2\frac{R(CH_2) - 1}{R(CH_2) + 2} \qquad f_{HS} = \frac{R(NH) - 1}{R(RH) + 2}$$

where $R = A_{//}/A_{\perp}$ is the dichroic ratio of the $\nu(CH_2)$ and δ(NH) absorption bands in the polarized spectra.

RESULTS AND DISCUSSION

When crystallized from the melt at 48 °C, the PEU forms ring-banded spherulite morphology, as shown in Figure 1. The spherulite exhibits Maltese cross and a distinct pattern of concentric rings under PLM, whereas under unpolarized light [Fig. 1(b)], the ring-banded structure is also clearly observed. The detailed morphology of these spherulites which were not able to be revealed by PLM[30] is further disclosed by AFM. Figure 2(a) gives an AFM height image of a typical ring-banded structure, and Figure 2(b) shows the height profile along the added black line in Figure 2(a). The above two figures reveal a clear ring-banded structure of the spherulite. It can be easily observed that the ringed bands are composed of alternating ridges and valleys. The band spacing is about 8 μm. Comparison of the AFM image with the PLM morphology reveals that the ring-banded spherulite consists of alternate convex and concave bands, and the dark and bright bands of the ring-banded spherulite under PLM [Fig. 1(a)] correspond to the convex and concave bands in the AFM image [Fig. 2(a)], respectively.

Figure 3(a) is the AFM image of the spherulite's convex band [area "a" in Fig. 2(a)] showing a sheet texture, and Figure 3(b) is a magnified view of the boxed region in Figure 3(a), showing a flat-on lamellae and layered terrace-like morphology. The lamellae thickness, measured from the height profile between the horizontal planes of the terrace-like lamellae, was ~7.8 nm based on multiple measurements over the spherulite. This thickness is consistent with that of PCL flat-on lamellae in the thin film.[43] Since PCL crystals have

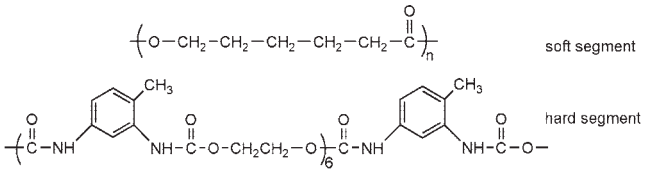

SCHEME 1 Chemical structure of the PEU.

orthorhombic unit cell, the chain (the c axis) is perpendicular to the substrate for flat-on lamellae.

Turning to the concave bands of the ring-banded spherulite, Figure 4(a,b) show the AFM images of the concave band magnified from the "b" area in Figure 2(a). The height image [Fig. 4(a)] with 4 × 4 μm^2 scan size shows the organization of the fibrils orienting along the radial direction of the spherulite. At a higher magnification, Figure 4(b) [1 × 1 μm^2 scan size, the box region of Fig. 4(a)] shows an almost parallel fibrillar texture that is made up of edge-on lamellae bundles. The width of the lamellae in the fibril is about 20 nm. Although not so accurate due to the broadening in the AFM measurements and interference of the surrounding fibrillar lamellae, this is consistent with that of the edge-on lamellae of PCL homopolymer formed in the presence of residual solvent.[44] The concave bands of banded spherulite are mainly composed of fibrillation of edge-on lamellae, which indicates that the PCL chains are parallel to the substrate plane.

We then used FTIR imaging, a convenient tool capable of combining spectral and spatial information for studying the morphology of semicrystalline polymers[39] to further analyze the orientation of PCL soft segments and hard segments in the ring-banded spherulite. Since the size of the spherulite was about 120 μm, an area of 256 × 256 μm^2 was studied. The CH_2 stretching and the NH deformation bands were selected to characterize the PCL soft segments and the hard segments, respectively, because these two are isolated bands without any overlapping and have high signal-to-noise ratio. The horizontal direction in the image was defined as the parallel direction, whereas the vertical the perpendicular direction, and the chain orientation function images of the PCL soft segments and the hard segments were constructed using the formula by a pixel-by-pixel calculation of the absorbance values from the parallel and perpendicular images. Figure 5(a) shows the orientation function image of the PCL soft segments, which can reveal the chain orientation within the spherulite. It can be seen that in the two horizontal sections (left and right), the orientation function values are negative, indicating that the chains orient perpendicular to the horizontal (parallel) direction, which is the tangential direction of the ring-banded spherulite. In the other two vertical sections (top and bottom), the values are positive, indicating that the chains are parallel to the horizontal direction. Thus, the FTIR imaging data show that in the entire spherulite, the PCL chains are perpendicularly oriented to the radial direction, which is consistent with the current knowledge on spherulites. Further information can be inferred by comparing the FTIR image with the corresponding AFM image of the spherulite. It can be seen that the orientation function values are very different in the concave and the convex bands. The orientation function values for the concave bands are very negative (about −0.40), and that for the convex bands are only slightly negative. This indicates that although the PCL chains are all perpendicular to the radial direction, they orient very differently in the concave and the convex bands with respect to the substrate plane. More specifically, the most PCL chains in the concave bands take parallel orientation to the substrate, while perpendicular orientation in the convex bands because the orientation function value is almost zero. These results are consistent with the AFM results discussed above. Since hard segments are in the amorphous phase, it is difficult to assess the orientation using traditional characterization techniques such as X-ray diffraction. FTIR imaging can be applied to analyze the dichroism of the amorphous chains and the orientation can then be deduced. Figure 5(b) shows the

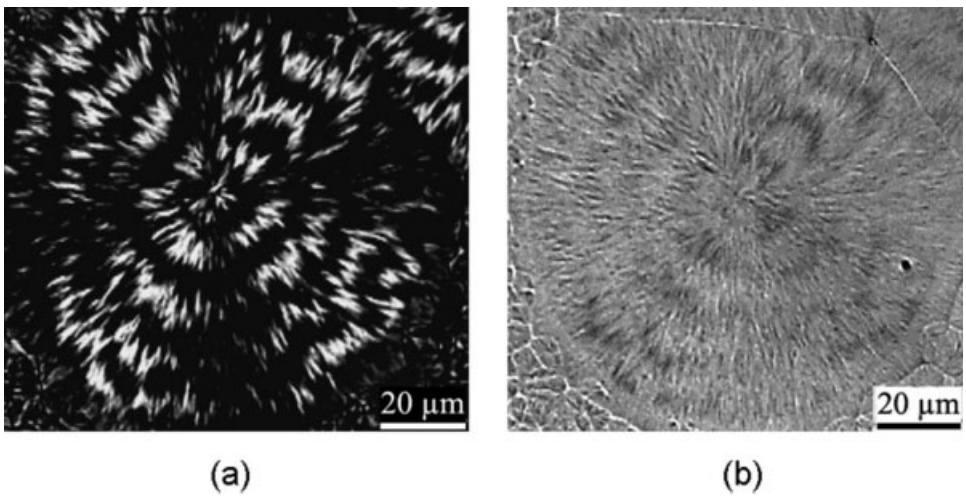

FIGURE 1 Optical micrographs of the PEU crystallized at 48 °C (a) under crossed-polarized light and (b) under unpolarized light.

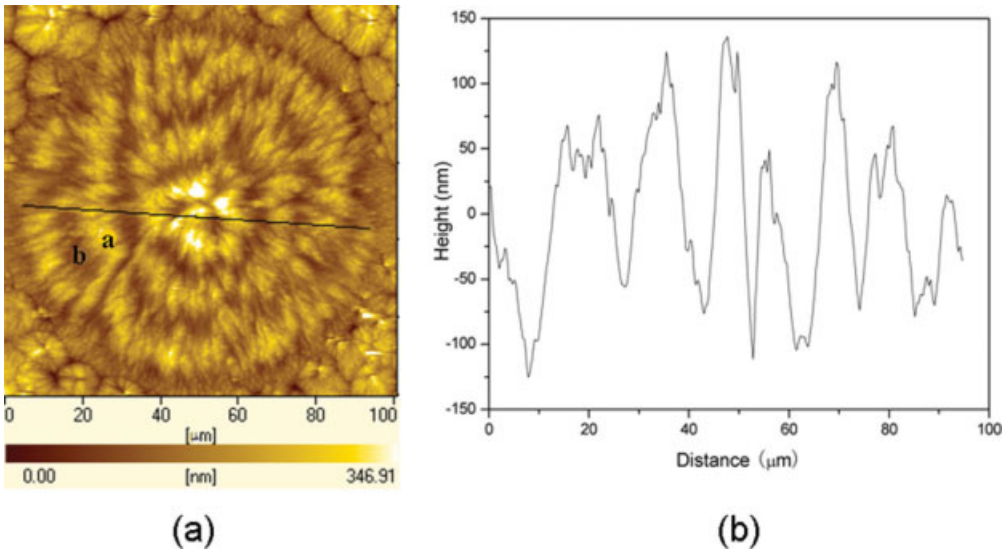

FIGURE 2 (a) AFM height image of the ring-banded spherulite and (b) the corresponding height profile along the added black line shown in (a). [Color figure can be viewed in the online issue, which is available at www.interscience.wiley.com.]

orientation function of the hard segments, which are almost zero throughout the whole ring-banded spherulite, indicating that the hard segments are oriented randomly throughout the whole spherulite.

What is the distribution of crystalline soft segment and amorphous hard segment in the ring-banded spherulite? This may be an important factor for the PEU forming ring-banded spherulites when crystallized from its melt. The distribution of the soft and the hard segments were investigated by FTIR imaging. To compensate for the thickness inhomogeneity within the selected area of the film, the PCL soft segment content was using the structure absorbance ratio $A_{\nu(CH2)}/A_{\delta(NH)}$, for $\nu(CH_2)$ is mainly from PCL soft segment and δ(NH) from hard segment, and the hard segment content was using the ratio $A_{\delta(NH)}/A_{\nu(CH2)}$. Figure 6(a) shows the optical image of the ring-banded spherulite, and it exhibits a distinct ring-banded structure as that under unpolarized light. Figure 6(b,c) shows the distribution of the contents of the PCL soft segments and the hard segments, and they both exhibit ring-banded structure. By comparing the content images with the AFM image of the spherulite, it is easy to conclude that the convex bands of the ring-banded spherulite are rich in PCL soft segments, and the concave bands are hard segment-rich regions.

Figure 7 shows the radius of the ring-banded spherulite as a function of crystallization time at 46 °C. The average growth rate is fitted from the experiment data with a slope of 0.035 μm/min for the convex bands and 0.010 μm/min for the concave bands, showing two distinct growth rates alternately appearing as the ring-banded spherulite grows. The specific growth rates associated to the convex and concave bands, which hints different growth mechanism

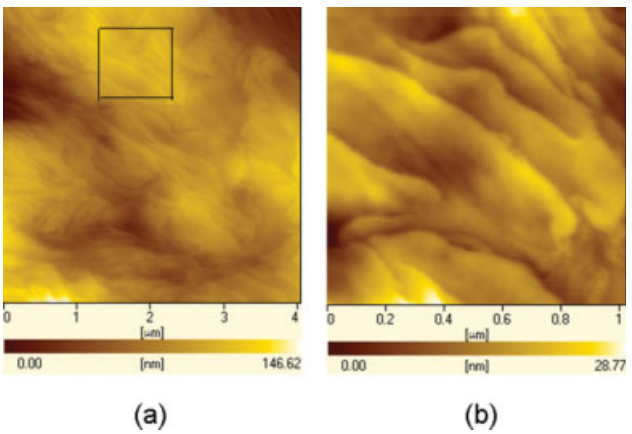

FIGURE 3 (a) AFM height image of the convex band of the ring-banded spherulite and (b) the magnification of the boxed region in (a). [Color figure can be viewed in the online issue, which is available at www.interscience.wiley.com.]

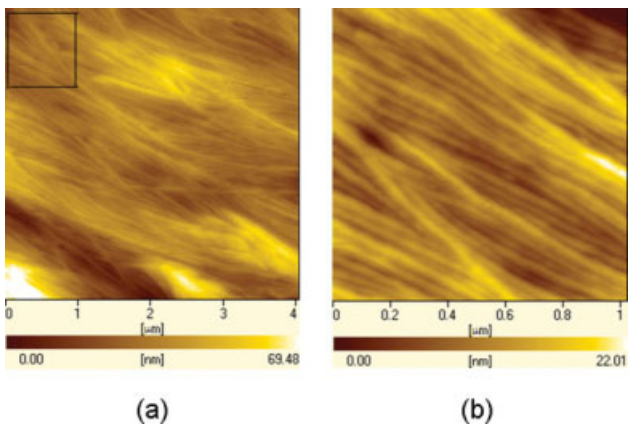

FIGURE 4 (a) AFM height image of the concave band of the ring-banded spherulite and (b) the magnification of the boxed region in (a). [Color figure can be viewed in the online issue, which is available at www.interscience.wiley.com.]

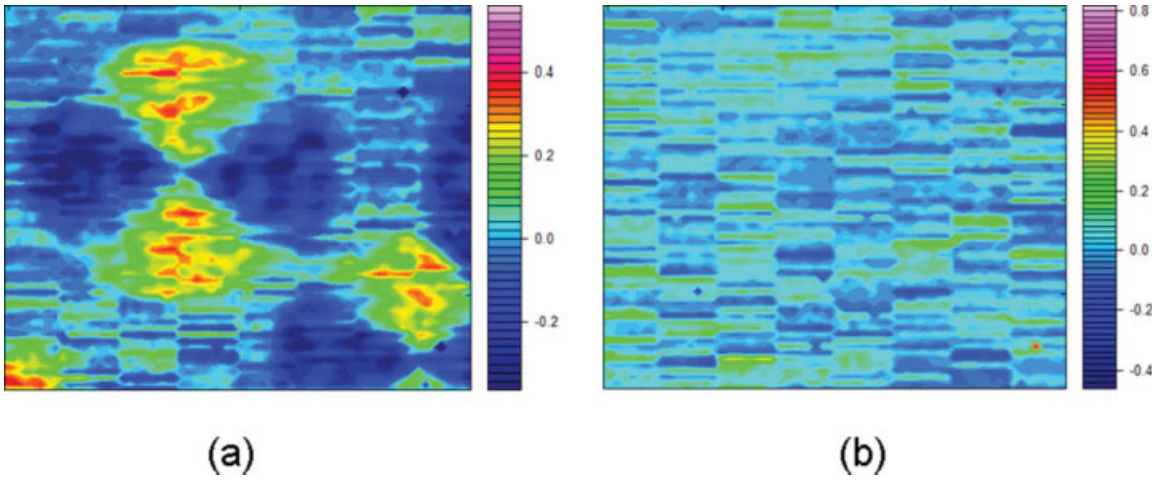

FIGURE 5 The corresponding orientation function images (256 × 256 μm^2) of (a) PCL soft segment (f_{SS}) and (b) hard segment (f_{HS}) with the added color scale.

between the two regions, give rhythmic growth character of the spherulite.[15,25,26,33]

The different orientations of the PCL soft segment chains in the convex and the concave bands may be due to the different growth mechanisms between the bands, and the composition field of the copolymer during crystallization. Scheme 2 schematically illustrates a possible mechanism for the formation of the ring-banded spherulite from the copolymer. The formation of the two bands is dictated by the different diffusion processes of the PCL chains during the crystallization from the melt. When the PCL chains diffuse forward, there are more crystallizable PCL chains in the frontal area, leaving less PCL chains in the posterior area. The PCL chains crystallize in the frontal area, forming convex band, whereas there

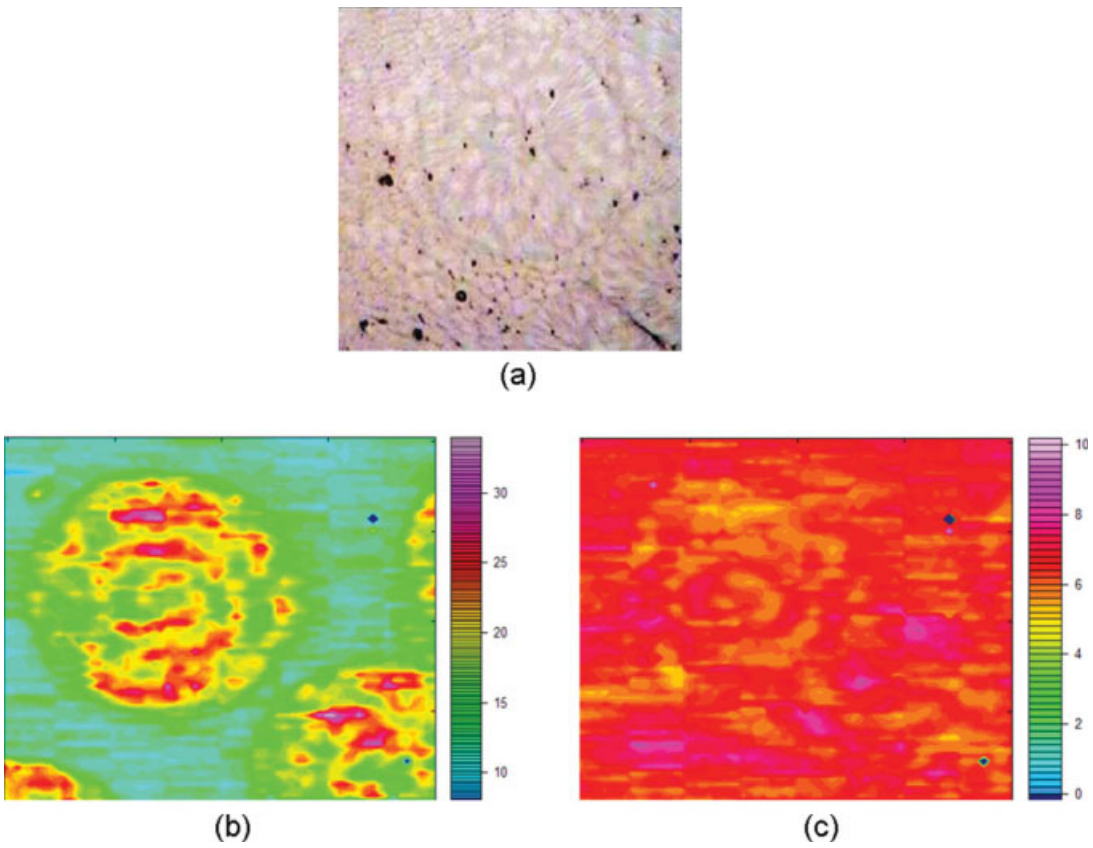

FIGURE 6 Optical image (a) and FTIR images (256 × 256 μm^2) showing the distribution of (b) PCL soft segment based on $A_{\nu(CH2)}/A_{\delta(NH)}$ and (c) hard segment based on $A_{\delta(NH)}/A_{\nu(CH2)}$ with the added color scale.

are hardly any PCL melt chains diffusing to the posterior area due to the hindering of the hard segments of high contents, and the crystallizable PCL segments in this area crystallize slowly due to the restriction of the hard segments and form the concave band. Then, this process is repeated and alternate convex and concave bands are formed in the whole spherulite, whereas the different chain orientations in the two bands may be caused by the different crystal growth mechanisms during the crystallization.

CONCLUSIONS

The ring-banded spherulite morphology of a multiblock PEU copolymer was investigated using PLM and AFM, and FTIR imaging was further employed to detail the composition distribution and chain orientation within these ring-banded spherulites. It was found that the convex bands of the ring-banded spherulites are mainly composed of PCL-rich domains, where PCL chains adopt perpendicular orientation to the substrate. The concave bands, however, are mainly enriched by the hard segments, where the orientation of PCL segments is parallel to the film plane but perpendicular to the radial growth directions of the spherulite. The different orientation of crystallizable PCL segment in-between convex and concave bands is attributed to the rhythmic growth mechanism during crystallization, as a consequence of composition distribution along the chains of the PEU copolymer.

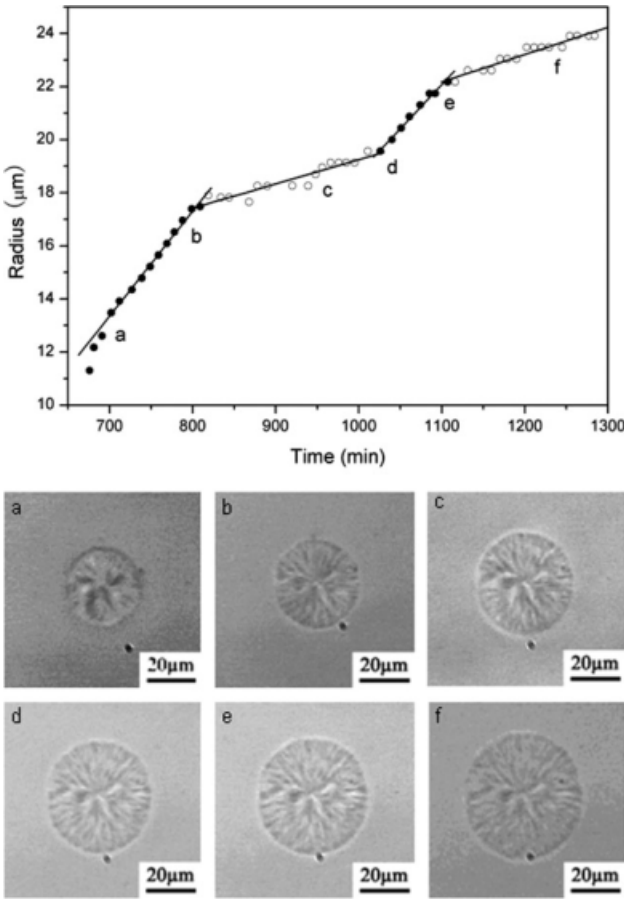

FIGURE 7 Rhythmic growth of ring-banded spherulite at T_c = 46 °C (●, convex band; ○, concave band). a–f are the optical images corresponding to the labels in the upper figure.

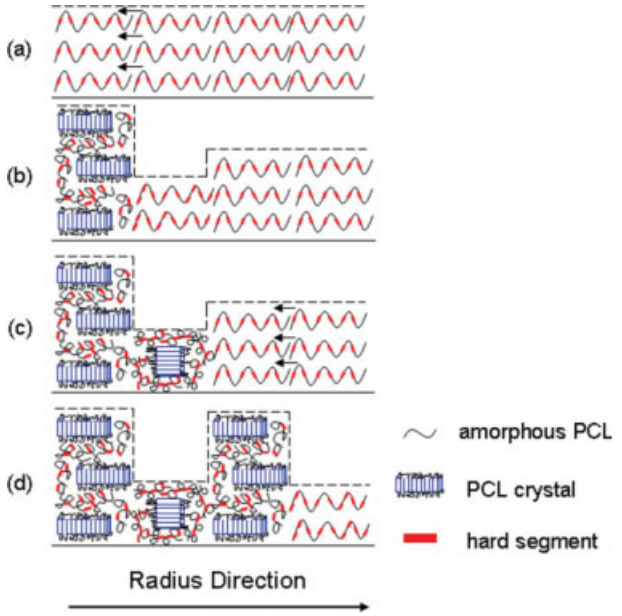

SCHEME 2 Model of the ring-banded spherulite formation. [Color figure can be viewed in the online issue, which is available at www.interscience.wiley.com.]

The authors thank X. Jing of CIAC for kindly providing the PEU sample for this work. The financial support from the National Natural Science Foundation of China (20423003, 20774097) is acknowledged. X. Yang and Z. Su thank the NSFC Fund for Creative Research Groups (50621302) for support.

REFERENCES AND NOTES

1 Ji, F. L.; Zhu, Y.; Hu, J. L.; Liu, Y.; Yeung, L. Y.; Ye, G. D. Smart Mater Struct 2006, 15, 1547–1554.

2 Lendlein, A.; Langer, R. Science 2002, 296, 1673–1676.

3 Metcalfe, A.; Desfaits, A. C.; Salazkin, I.; Yahia, L.; Sokolowski, W. M.; Raymond, J. Biomaterials 2003, 24, 491–497.

4 Wache, H. M.; Tartakowska, D. J.; Hentrich, A.; Wagner, M. H. J Mater Sci Mater Med 2003, 14z, 109–112.

5 Behl, M.; Lendlein, A. Soft Matter 2007, 3, 58–67.

6 Lendlein, A.; Jiang, H. Y.; Junger, O.; Langer, R. Nature 2005, 434, 879–882.

7 Ping, P.; Wang, W. S.; Chen, X. S.; Jing, X. B. Biomacromolecules 2005, 6, 587–592.

8 Lee, B. S.; Chun, B. C.; Chung, Y. C.; Sul, K. I.; Cho, J. W. Macromolecules 2001, 34, 6431–6437.

9 Lendlein, A.; Kelch, S. Angew Chem Int Ed 2002, 41, 2034–2057.

10 Behl, M.; Lendlein, A. Mater Today 2007, 10, 20–28.

11 Liu, C.; Qin, H.; Mather, P. T. J Mater Chem 2007, 17, 1543–1558.

12 Beloshenko, V. A.; Varyukhin, V. N.; Voznyak, Y. V. Russian Chem Rev 2005, 74, 265–283.

13 Wang, W. S.; Ping, P.; Chen, X. S.; Jing, X. B. Eur Polym J 2006, 42, 1240–1249.

14 Ji, F. L.; Hu, J. L.; Li, T. C.; Wong, Y. W. Polymer 2007, 48, 5133–5145.

15 Wang, Z. G.; An, L. J.; Jiang, B. Z.; Wangh, X. H. Macromol Rapid Commun 1998, 19, 131–133.

16 Cheung, Z. L.; Weng, L. T.; Chan, C. M.; Hou, W. M.; Li, L. Langmuir 2005, 21, 7968–7970.

17 Su, C. C.; Lin, J. H. Colloid Polym Sci 2004, 283, 182–193.

18 Xiao, Q.; Yan, S.; Rogausch, K. D.; Petermann, J.; Huang, Y. J Appl Polym Sci 2001, 80, 1681–1686.

19 Jiang, S. C.; He, C. L.; An, L. J.; Chen, X. S.; Jiang, B. Z. Macromol Chem Phys 2004, 205, 2229–2234.

20 Bisault, J.; Rysschenkow, G. J Cryst Growth 1991, 110, 889–909

21 Hutter, J. L.; Bechhoefer, J. J Cryst Growth 2000, 217, 332–343.

22 Lotz, B.; Cheng, S. Z. D. Polymer 2005, 46, 577–610.

23 Keller, A. J Polym Sci 1959, 39, 151–173.

24 Keith, H. D.; Padden, F. J. Macromolecules 1996, 29, 7776–7786.

25 Kyu, T.; Chiu, H. W.; Guenthner, A. J.; Okabe, Y.; Saito, H.; Inoue, T. Phys Rev Lett 1999, 83, 2749–2752.

26 Okabe, Y.; Kyu, T.; Saito, H.; Inoue, T. Macromolecules 1998, 31, 5823–5829.

27 Wang, Z. B.; Alfonso, G. C.; Hu, Z. J.; Zhang, J. D.; He, T. B. Macromolecules 2008, 41, 7584–7595.

28 Toda, A.; Okamura, M.; Taguchi, K.; Hikosaka, M.; Kajioka, H. Macromolecules 2008, 41, 2484–2493.

29 Chao, C. C.; Chen, C. K.; Chiang, Y. W.; Ho, R. M. Macromolecules 2008, 41, 3949–3956.

30 Wang, Y.; Chan, C. M.; Li, L.; Ng, K. M. Langmuir 2006, 22, 7384–7390.

31 Duan, Y. X.; Jiang, Y.; Jiang, S. D.; Li, L.; Yan, S. K.; Schultz, J. M. Macromolecules 2004, 37, 9283–9286.

32 Fromsdorf, A.; Woo, E. M.; Lee, L. T.; Chen, Y. F.; Forster, S. Macromol Rapid Commun 2008, 29, 1322–1328.

33 Chuang, W. T.; Hong, P. D.; Chuah, H. H. Polymer 2004, 45, 2413–2425.

34 Xu, J.; Guo, B. H.; Zhang, Z. M.; Zhou, J. J.; Jiang, Y.; Yan, S.; Li, L.; Wu, Q.; Chen, G. Q.; Schultz, J. M. Macromolecules 2004, 37, 4118–4123.

35 Ikehara, T.; Jinnai, H.; Kaneko, T.; Nishioka, H.; Nishi, T. J Polym Sci Part B: Polym Phys 2007, 45, 1122–1125.

36 Jiang, Y.; Zhou, J. J.; Li, L.; Xu, J.; Guo, B. H.; Zhang, Z. M.; Wu, Q.; Chen, G. Q.; Weng, L. T.; Cheung, Z. L.; Chan, C. M. Langmuir 2003, 19, 7417–7422.

37 Gazzano, M.; Focarete, M. L.; Riekel, C.; Scandola, M. Biomacromolecules 2000, 1, 604–608.

38 Tanaka, T.; Fujita, M.; Takeuchi, A.; Suzuki, Y.; Uesugi, K.; Doi, Y.; Iwata, T. Polymer 2005, 46, 5673–5679.

39 Snively, C. M.; Koenig, J. L. J Polym Sci Part B: Polym Phys 1999, 37, 2353–2359.

40 Chernev, B.; Wilhelm, P. Monatsh Chem 2006, 137, 963–967.

41 Bhargava, R.; Wang, S. Q.; Koenig, J. L. Adv Polym Sci 2003, 163, 137–191.

42 Vogel, C.; Wessel, E.; Siesler, H. W. Macromolecules 2008, 41, 2975–2977.

43 Mareau, V. H.; Prud'homme, R. E. Macromolecules 2005, 38, 398–408.

44 Mareau, V. H.; Prud'homme, R. E. Polymer 2005, 46, 7255–7265.